



HAL
open science

SIZE NUCLEI MEASUREMENT IN A CAVITATION TUNNEL BY DIGITAL IN-LINE HOLOGRAPHY

D. Lebrun, D. Allano, F. Walle, F. Corbin, L. Méès, D. Fréchou, R. Boucheron

► **To cite this version:**

D. Lebrun, D. Allano, F. Walle, F. Corbin, L. Méès, et al.. SIZE NUCLEI MEASUREMENT IN A CAVITATION TUNNEL BY DIGITAL IN-LINE HOLOGRAPHY. 2nd International Conference on Advanced Model Measurement Technology for EU Maritime Industry (AMT'11), Apr 2011, Newcastle upon Tyne, United Kingdom. hal-02414441

HAL Id: hal-02414441

<https://hal.science/hal-02414441>

Submitted on 16 Dec 2019

HAL is a multi-disciplinary open access archive for the deposit and dissemination of scientific research documents, whether they are published or not. The documents may come from teaching and research institutions in France or abroad, or from public or private research centers.

L'archive ouverte pluridisciplinaire **HAL**, est destinée au dépôt et à la diffusion de documents scientifiques de niveau recherche, publiés ou non, émanant des établissements d'enseignement et de recherche français ou étrangers, des laboratoires publics ou privés.

SIZE NUCLEI MEASUREMENT IN A CAVITATION TUNNEL BY DIGITAL IN-LINE HOLOGRAPHY

D. Lebrun, D. Allano, F. Walle, F. Corbin, UMR 6614 CORIA, Avenue de l'Université, 76801 Saint-Etienne du Rouvray, France

L. Méès, LMFA – UMR CNRS 5509, Ecole centrale de Lyon, 69134 Ecully Cedex, France

D. Fréchou, R. Boucheron, Techniques Hydrodynamiques, (formerly Bassin d'essai des carènes), 27100 Val-de-Reuil, France

Digital in-line Holography (DIH) is used to measure size and concentration of small bubbles (6-100 μm) in hydrodynamic facilities. The forward diffraction pattern produced by small objects (bubbles, droplets, particles) illuminated by a laser diode is directly recorded by a camera without objective lens. From this pattern, each image plane can be reconstructed by applying back-propagation formalism (Huygens-Fresnel Integral). Then, after having reconstructed the whole volume, the 3-D location and size of each particle can be measured. Here the wavelet transform is used for the implementation of Fresnel Integral.

In the present case, nuclei are measured by a sampling probe specially designed for DIH measurements and equipped with transparent sections. A diverging beam coming from a fiber coupled laser diode ($\lambda=635\text{ nm}$, $P=12\text{ mW}$) illuminates the sample volume and the hologram is recorded by a 1280×1024 CMOS camera. From each hologram the volume can be reconstructed slice by slice. We present here the method used for obtaining the size nuclei distribution extracted from hologram analysis. Statistical results (5000 holograms are recorded and processed) obtained under different pressures ($P=567, 927$ and 1287 mbars) are compared and discussed.

1. Introduction

Digital in-line holography (DIH) can be efficiently used for particle diagnostics in small volumes. When a magnification is wanted, particles images can be imaged close to the camera by using a couple of lenses for obtaining a magnification higher than 1 during the reconstruction stage. Such systems are interesting when the 2D sensor (CCD or CMOS camera) cannot be placed near the sample to be studied [1]. In more convenient situations a magnification factor can also be directly obtained by illuminating the sample volume with a diverging beam coming from a pinhole or a laser coupled in an optical fiber. This enables to spread the diffraction pattern over a larger area. Furthermore, the image sensor can be brought closer to the objects to be recorded. Consequently, the numerical aperture (NA) of the recording system is increased and a significant magnification of the reconstructed images is observed. Numerous papers have been published under this configuration also called Digital In-line Holographic Microscopy (DIHM). For example, the authors of Ref. [2] have shown that a resolution of order of the wavelength can be reached. Two decades ago, Vikram et al. [3] studied the gain obtained by recording the holograms with a divergent beam. Under far-field condition (i.e. when the object size d verifies the inequality $\frac{\pi d^2}{\lambda z_e} \ll 1$, where z_e is the recording distance), the authors of Ref. [3] concluded that the

problem can be exactly formulated as if the hologram were recorded with a plane wave. In other terms, the equation describing intensity distribution in the camera is nothing but the intensity distribution of

an equivalent magnified object recorded at an equivalent magnified distance from the camera. As a result, digital holograms can be simply processed as a common in-line hologram that would have been recorded with a collimated plane wave. This configuration is used here to measure the size and position of small bubbles in a cavitation tunnel. Thus, the size distribution obtained from thousands of holograms can be estimated under different pressures. The objective of this communication is to describe the method used for choosing the best configuration of the diverging recording wave in the diameter range (5-140 μm) . In Section 2, the expression of the intensity recorded by holograms is recalled and the resulting magnification factor is expressed. Here the hologram pattern is sampled by a digital camera (CMOS). This means that the spatial sampling conditions must be checked. According to this sampling constraint, the discussions of Section 3 lead to the optimal curvature radius of the recording wave that is needed for obtaining the wanted spatial resolution in the reconstruction image plane. The digital hologram reconstruction principle is recalled in section 4. A transparent pipe has been specially designed for recording holograms of nuclei collected from the cavitation tunnel. The experimental setup and the diameter measurement method are described in sections 5 and 6. Here, statistical results are expected and thousands of holograms have been recorded leading to an enormous volume of data (100 Mbytes/hologram). The automatic processing of holograms and the measured size distributions are described in section 7 and a conclusion is given in section 8.

2. Digital holography with a spherical recording wave

The optical configuration of in-line holography is given by figure 1. A single laser beam coming from a point source S illuminates the particle and a 2D detector records the interferences produced by the superposition of the direct beam and the wave scattered by the bubble. The point source and the object are located respectively at the distances z_s and z_e from the camera.

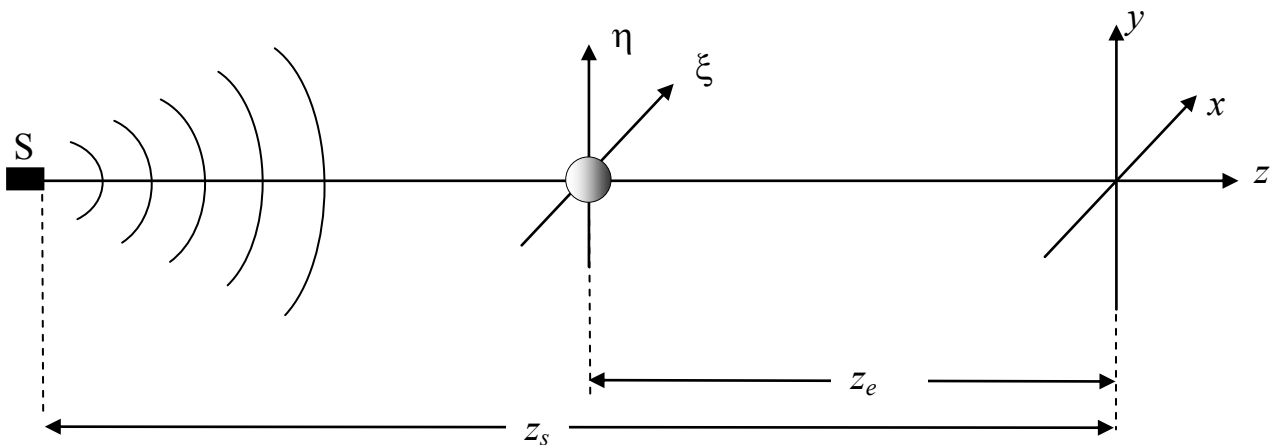


Fig. 1 – Optical configuration of recording in-line holograms of bubbles with a divergent beam. S : Laser source, (ξ, η) : object plane (x, y) : 2D detector plane

Consider that the input function in the (ξ, η) plane is :

$$A_0(\xi, \eta) = (1 - O) e^{i\pi \frac{(\xi^2 + \eta^2)}{\lambda(z_s - z_e)}} \quad (1)$$

Under Fresnel approximation, the amplitude distribution in the (x, y) plane is [4] :

$$A_{z_e}(x, y) = \frac{e^{\frac{2i\pi}{\lambda z_e}}}{i\lambda z_e} \iint (1 - O) e^{i\pi \frac{(\xi^2 + \eta^2)}{\lambda(z_s - z_e)}} e^{i\pi \frac{(x - \xi)^2 + (y - \eta)^2}{\lambda z_e}} d\xi d\eta \quad (2)$$

Assuming that the far-field conditions are checked $\left(i.e. \frac{\pi(\xi^2 + \eta^2)}{\lambda z_e} \ll 1 \right)$, a spherical object can be approximated by an opaque disk of diameter d . By introducing $r = \sqrt{x^2 + y^2}$, and by omitting the constant phase term $e^{\frac{2i\pi}{\lambda z_e}}$, the calculus of integral (2) gives [4] :

$$A_{z_e}(r) = 1 - \lambda K z_e e^{-i\frac{\pi}{2}} e^{\frac{i\pi r^2}{K\lambda z_e}} F_d \frac{(r)}{\lambda z_e} \quad (3)$$

where

$$F_\alpha(r) = \frac{\pi}{2} \alpha^2 \frac{J_1(\alpha)}{\alpha} \quad (4)$$

and

$$K = \frac{z_s}{z_s - z_e} \quad (5)$$

The intensity distribution in the camera plane is deduced from (3) by the relation $I_{z_e}(r) = A_{z_e}(r) \overline{A_{z_e}(r)}$ where $\overline{\cdot}$ denotes the complex conjugate :

$$I_{z_e}(r) = 1 - 2\lambda K z_e \sin\left(\frac{\pi r^2}{\lambda K z_e}\right) F_d \frac{(r)}{\lambda z_e} + (\lambda K z_e)^2 F_d^2 \frac{(r)}{\lambda z_e} \quad (6)$$

By defining the equivalent variables $z_{eq} = K z_e$, and $d_{eq} = K d$, $I_{z_e}(r)$ can be simply rewritten as follows :

$$I_{z_e}(r) = 1 - 2\lambda z_{eq} \sin\left(\frac{\pi r^2}{\lambda z_{eq}}\right) F_{\frac{d_{eq}}{\lambda z_{eq}}}(r) + (\lambda z_{eq})^2 F_{\frac{d_{eq}}{\lambda z_{eq}}}^2(r) \quad (7)$$

As a result, a single equation is sufficient to describe the intensity distribution of a particle hologram whatever the divergence of the recording beam. K can be seen as a magnification factor and is a function of the distance object camera z_e .

In other words, equation (7) shows that the diffraction pattern produced by an object of diameter d illuminated by a spherical wave with a curvature radius z_s and recorded at a distance z_e can be simply expressed as the intensity distribution produced by an object of diameter Kd illuminated by a plane wave and located at a distance Kz_e from the camera.

This result is very convenient because it lead to a very simple way for the processing of digital holograms. It means that the diffraction pattern of a given object can be processed exactly as if the hologram were recorded with a plane wave and all the conditions (spatial sampling, recording distance, spatial resolution) can be expressed in the equivalent magnified space. This point will be developed in sections 3 and 4.

Note that the magnification factor K can also be written as a function of z_{eq} by replacing z_e by z_{eq}/K in equation (5):

$$K = \frac{z_s + z_{eq}}{z_s} \quad (8)$$

3. Hologram recording conditions

3.1. Spatial sampling

Classically, in digital holography the sampling conditions need at least 2 pixels of size p per fringe period. When this condition is not checked, it may give rise to moiré effects and an optical low-pass filter should be applied before spatial sampling the diffraction pattern [5]. In order to avoid such unwanted effects, the angle between the recording wave and the object wave must be lower than $2\arcsin\left(\frac{\lambda}{4p}\right)$ [6]. Considering the case where a centred particle is recorded with a plane wave, the

above condition can be approximated by $\theta_{\max} \approx \frac{\lambda}{p}$ where θ_{\max} is the maximum collecting angle by the camera (i.e. angle viewed from the object). For a digital camera composed of $N \times N$ pixels, this condition is easily checked when the recording distance z_e is higher than an optimal distance equal to

$$\frac{Np^2}{\lambda} [7,8].$$

In the present work, a diverging beam is used. Thus, the above condition must not applied to the working distance z_e but to the equivalent distance $z_{eq} = Kz_e$. It follows that the sampling condition leads to $Kz_e > \frac{Np^2}{\lambda}$. By using the definition of K (equation (5)), the recording distance z_e should respect the following inequality:

$$z_e > \frac{Np^2}{\lambda} \left(1 + \frac{Np^2}{\lambda z_s} \right)^{-1}. \quad (9)$$

Eq. (9) shows the conditions needed for a convenient spatial sampling of the interference fringes by the camera when an object is illuminated by a spherical wave.

This result also means that by using a diverging beam (*i.e.* by decreasing the value of z_s), the camera can be moved closer to the studied objects without braking in the spatial sampling conditions. As a result, the numerical aperture (NA) can be increased and smaller objects can be studied. This point is detailed in the next subsection.

3.2. Spatial resolution

From authors of ref [2], the spatial resolution is δ related to the numerical aperture (NA) of the hologram. It can be given by the ratio $\delta = \lambda / (2NA)$ where $NA = (Np/2) \left[(Np/2)^2 + z_e^2 \right]^{1/2}$. The highest NA is obtained for the optimal recording optimal distance $z_{opt} = \frac{1}{K} \frac{Np^2}{\lambda}$. Then, we deduce the best spatial resolution that can be expected for a given magnification factor K :

$$\delta = \frac{p}{K} \sqrt{1 + \left(\frac{K\lambda}{2p} \right)^2} \quad (10)$$

The sampling step is generally much greater than the product $K\lambda$. Consequently, equation (10) shows that the spatial resolution is roughly improved by a $1/K$ factor with a divergent beam.

Note also that in the optimal case as regards to the sampling condition (*i.e.* $z_e = z_{opt}$), equation (5) gives the optimal distance source-camera z_s that should be used for a given magnification K :

$$z_s = \frac{Np^2}{(K-1)\lambda} \quad (11)$$

For example, if a 1024×1024 camera with $p = 6.7 \mu m$ illuminated by a laser of wavelength $\lambda = 635 nm$ is used, equation (11) indicates that the distance source-sensor must be lower to a limit distance $z_s = 72.4 mm$ for safely recording holograms with a magnification K higher than 2.

3.3. Case of DIH with a relay lens

Another way for magnifying holographic particle images is to use a relay lens. Let us describe the case where an object is illuminated by a plane wave and imaged near the CCD sensor by using an objective lens with a focal length f . This configuration, not used in the present case, is shown in figure II.

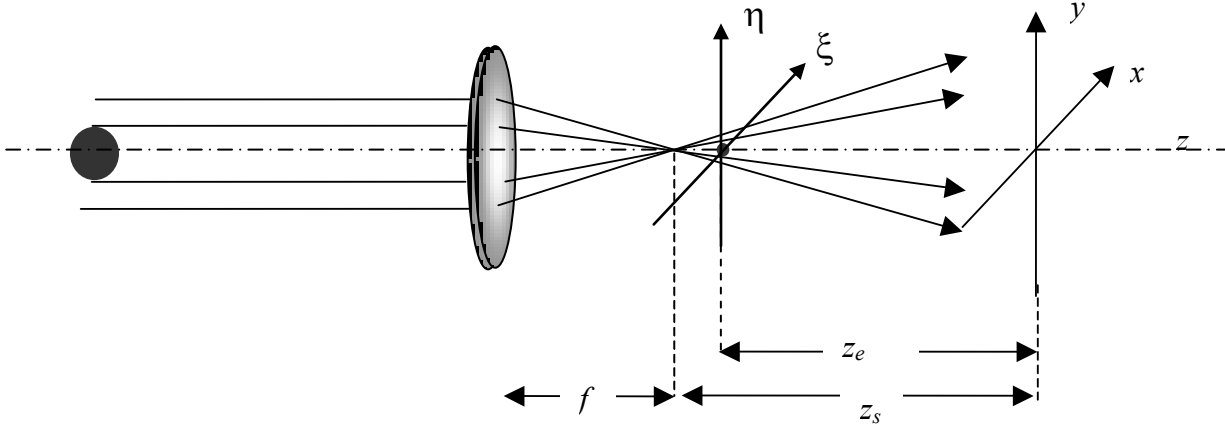


Fig. II – Optical configuration of recording in-line holograms with an imaging lens

With this configuration, assuming that well-known geometrical optics laws can be used, a given object is imaged in the (ξ, η) plane with the magnification:

$$\gamma = -\frac{z_s - z_e}{f} . \quad (12)$$

This geometric image can be considered as an object placed in a diverging beam coming from the focal point. As a result, using the conclusions of section 2, the intensity distribution recorded on the (x, y) plane can be seen as the diffraction pattern produced by a magnified object (of factor K) illuminated by a plane wave. The resulting magnification is simply given by the product $K\gamma$. By using (5) and (12), the total magnification is rewritten:

$$K\gamma = -\frac{z_s}{f} \quad (13)$$

Consequently, if we assume that the far-field conditions are fulfilled, the holographic magnification given by the curvature radius counterbalances exactly the geometrical magnification given by an imaging lens. Therefore, the total magnification is not dependent on the axial location of the objects z_e but depends only on the ratio $\frac{z_s}{f}$. The 3D particle volume can be reconstructed and analyzed without

introducing any correction factor. This result is in good accordance with the formulation given in Ref [9] for Digital holographic microscopy. Although this configuration offers the advantage of invariance of the magnification, we have preferred to directly illuminate the objects by a diverging beam (see Fig.

I). In this way, the number of optical elements is reduced and geometrical aberrations, often observed when a microscope objective is used, are avoided.

4. Reconstruction of magnified particle images

As said in section 2, the holograms are processed as if they were recorded by a plane wave. Let us recall the principle of the recording and reconstruction of digital holograms. Consider a particle located at a distance z_e from the recording plane. Under far-field approximation, the intensity distribution recorded by the camera can also be described by the following convolution:

$$I_{z_e}(x, y) = 1 - \left[O ** \left(h_{z_e} + \overline{h_{z_e}} \right) \right] (x, y) \quad (14)$$

where $I - O(x, y)$ is the object transmission function (here a bubble) and $h_{z_e}(x, y) = \frac{1}{i\lambda z_e} \exp\left[i \frac{\pi}{\lambda z_e} (x^2 + y^2) \right]$ the Fresnel Kernel.

As for the recording step, the intensity distribution in a reconstructed image located at a distance z_r from the camera is also calculated by a convolution operation:

$$R(x, y) = \left[I_{z_e} ** \left(h_{z_r} + \overline{h_{z_r}} \right) \right] (x, y) \quad (15)$$

It is easy to show that when the best focus plane is reached (i.e. when $z_r = z_e = z$), we obtain :

$$R(x, y) = 2 \left\{ 1 - O(x, y) - \frac{1}{2} \left[O(x, y) ** \left(h_{2z} + \overline{h_{2z}} \right) \right] (x, y) \right\} \quad (16)$$

As shown by eq (16), the reconstructed image $I - O(x, y)$ is surrounded by the unwanted fringes $\frac{1}{2} O(x, y) ** \left(h_{2z} + \overline{h_{2z}} \right) (x, y)$. In our case (far-field conditions), this fringes due to the « twin image » located at a distance $2z$ does not disturb the particle image. The wavelet method described in Ref.10 has been used for implementing the calculation of $R(x, y)$ (see subsection 6.1).

5. Experimental setup

The system used for recording holograms is shown on figure III. The sample volume is illuminated by a diverging beam coming from a single mode optical fiber with a $5 \mu\text{m}$ core. The source is a modulated laser diode emitting at $\lambda = 635 \text{ nm}$. The image sensor is a 1280×1024 CMOS camera with $6.7 \mu\text{m}$ pixels. The curvature radius (taking into account that the wave passes through media of different indices) is set to $z_s = 79.7 \text{ mm}$, leading from eq. (11) to an optimal magnification $K = 1.9$.

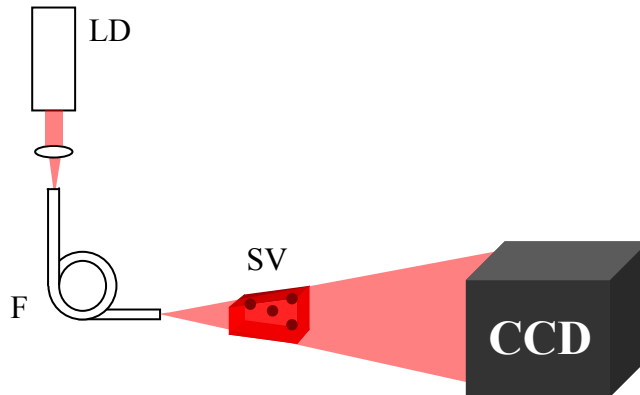


Fig. III – Hologram recording for size nuclei measurement. CCD : Camera, LD :modulated laser diode, F : single mode optical fiber, SV : Sample volume.

Note that a direct measurement in the hydrodynamic test section (cross section of $2m \times 1,35m$) would have been difficult. Then, an optical probe has been specially designed for these tests. The flow sampling hydraulic loop includes an optical pipe which has an internal square section in order to have two planar optical perpeX windows (see fig. IV). A cylindrical pipe, which would have been easier to manufacture, could have been used for these tests. However, the processing of digital holograms is not straightforward even if we have shown that the Fractional Fourier Transform has to be used in this case to reconstruct images [11].

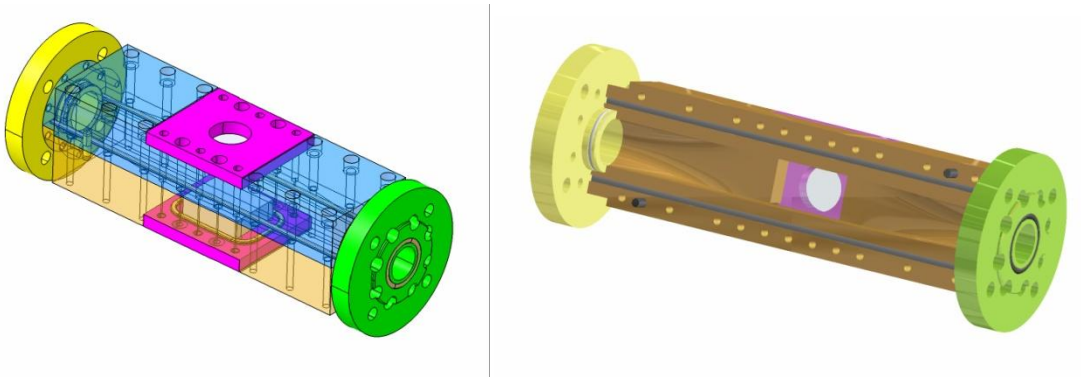


Fig. IV – Optical pipe used for digital holography

With this experimental setup, more than 5000 holograms have been recorded with 3 different flow pressures ($P=567$ mb, $P=927$ mb and $P=1287$ mb). The recording conditions are summarized in tab. I

Tab. I – Hologram recording conditions

Power of the laser source	12 mW
Beam divergence	250 mrad
Wavelength	635 nm
Curvature radius z_s	79.7 mm
Image size to be processed	1024x1024 pixels
Image recording rate	5 Hz
Pulse duration	10 μ s
Depth of the sample volume, range [5-25 μ m]	6 mm
Depth of the sample volume, range [12-140 μ m]	30 mm
Total measurement volume	59 mm ³
Magnification range through the sample volume	$2.13 < K < 4.5$

6. Holograms processing

6.1. Influence of the wavelet aperture

Each hologram is reconstructed plane by plane by applying by a Gaussian shape wavelet formalism described in ref. [10]. This enables to adapt the working aperture θ for hologram reconstruction and leads to an extended the depth of diameter measurement. Indeed, when a collimated beam is used ($K=1$), the authors of reference [12], have shown that the point-spread function is invariant in the 3D space and its width is theoretically equal to $L_{th} = \frac{2.3\lambda}{\theta}$. Here, the aperture has been reduced to $\theta = 55 \text{ mrad}$ leading to $L_{th} = 27 \mu\text{m}$ over the whole depth of the sample volume. This signifies that the object diameter is related to the image diameter by a single theoretical curve. The simulations of Figure V(a) show the correspondence between the object and the measured image size for small particles when the working aperture $\theta = 55 \text{ mrad}$ is selected.

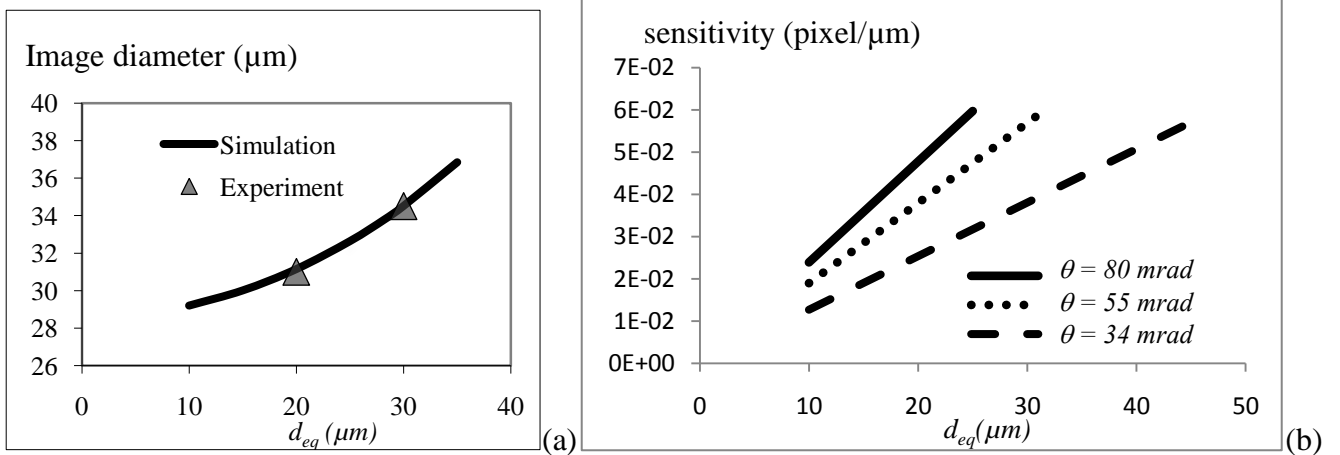


Fig. V– Influence of the wavelet aperture θ on diameter measurement in the equivalent space (plane wave configuration) (a) Simulated reconstructed image diameter versus equivalent object diameter, $\theta = 55 \text{ mrad}$, (b) sensitivity of diameter measurement for different working apertures

Note here that for smallest objects, the image diameter becomes invariant and tends toward a limit image diameter (slightly higher than L_{th}).

This observation is confirmed by Fig. V(b) where the predicted sensitivity (image size evolution for a increasing of 1 μm of the object size) is plotted versus the object diameter for different wavelet apertures. This graph shows that by selecting $\theta = 55\text{mrad}$ it is would be possible to build a histogram of particle diameter by step of 4 μm , provided that the image size can be estimated with an accuracy of 0.08 pixel.

Here, it must be recalled that the graphs of Figure V have been plotted in the equivalent space (plane wave configuration) mentioned in section 2. Moreover, we have shown that a particle image can be measured with accuracy better than 0.1 pixel. Thus, knowing that the magnification K is higher than 2 (see tab I), a classification of nuclei by intervals of 2 μm in the diameter range [5-25 μm] can be expected.

6.2. Focusing

The method used for searching the best focus plane depends on the diameter range that is investigated. For the range (5-25 μm), the z -coordinate of a particle image (z_{eq}), has been estimated by searching the reconstructed plane that leads to a maximum image contrast. However, as described in [13], this criterion is not valid for big particles and the Bexon method has been used for the focusing the biggest particles of the upper range (12-140 μm) [14]. It must be noted that the density of small bubbles is two orders of magnitude higher than the density of bigger bubbles. This is the reason why the size of the interrogation volume has been adapted for each diameter range (see tab. I).

Figure VI gives an example of bubbles reconstructed under this configuration. As described in section 2, equation (8) gives the correction factor K that must be applied to z_{eq} for recovering the right axial coordinate z_e in the sample volume. Note also the background disturbance surrounding the image of small bubble. It is commonly admitted that a particle image have to be reconstructed with a signal-to-noise ratio (SNR) higher 5 [15,16]. Here we have removed particle images under 8dB (SNR=6.3). This fixes the lower limit of detection.

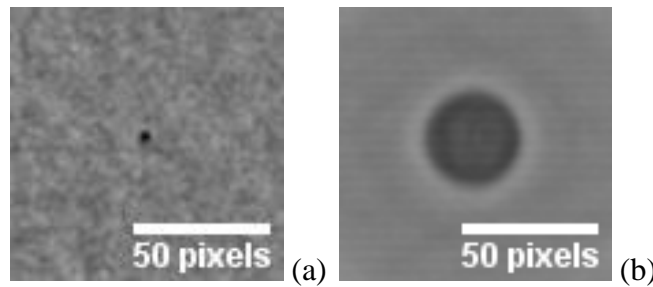


*Fig. VI – Example of image bubble reconstructed at different depth.
(a) $z_e = 44\text{ mm}$ ($d=10\ \mu\text{m}$), (b) $z_e = 50\text{ mm}$ ($d=85\ \mu\text{m}$)*

For the configuration presented in this paper, the depth location of each bubble is known with an accuracy better than 0.1 mm. For this study, all the particles have been located within a measurement volume $V_{meas} = 59\text{ mm}^3$

6.3. Diameter measurement and calibration of the technique

From the best focus reconstructed plane, the particle size is simply determined by counting the pixels whose grey-level are below a 50% threshold [13]. After having estimated the diameter d_{eq} , the magnification factor K (that depends on the depth coordinate z_{eq}) is applied to estimate the actual particle diameter. The curvature radius of the recording wave is z_s , evaluated by using the known distance separating the input and output planar optical window. The estimation of this distance by holography leads to a satisfactory knowledge of the axial magnification ratio. The sizing method has been calibrated on particle images reconstructed by simulated holograms in the range of [5-140 μm]. Then, this method has been validated by using a particle size standard composed of 27 opaque disks deposited by a microlithography technique on a quartz substrate in the range [2 μm , 1000 μm]. Fig. Va shows that the experimental measured diameters are in good accordance with the simulations for diameters d_{eq} of 20 and 30 μm . For higher diameters, we have shown that the particle diameter d_{eq} can be measured with an accuracy better than 10% in the range [40-200 μm].

7. Automatic processing of holograms and experimental results

After having recorded holograms in-situ (Facilities of Techniques Hydrodynamiques, formerly Bassin d'Essai des Carènes), the post-processing is realized at CORIA laboratory. Here, 5000 holograms have been processed by a fully automatic process developed at CORIA. The computational time needed for extracting the 3D location and size of nuclei is about 2 min/hologram with a 8 processors computer. The results for each pressure condition in the tunnel and for both nuclei diameter range are presented in tab. II.

Tab. II – Particle detected in the lower and upper range

Pressure	P=567 mb	P=927 mb	P=1287 mb	TOTAL
Number of holograms	1000	2000	2000	5000
Number of particles in the range [5-25 μm]	1175	2245	2257	5677
Number of particles in the range [12-140 μm]	37	70	71	178

The processing method and the results are summarized in the following subsections.

7.1. Range 6-25 μm

The reliability of diameter measurement is strongly dependent on the capability of depth-coordinate estimation. As described in [12], the 3D invariance of the PSF is only applicable when the particle image is well-focused. However, it has been shown in ref. 13, that the focusing problem is easy to solve in the range [5-25 μm]. In that case, the depth coordinate is estimated with accuracy better than 100 μm . The size distribution over this range is presented on fig. VII. Note that the results are quite similar for the three pressures conditions.

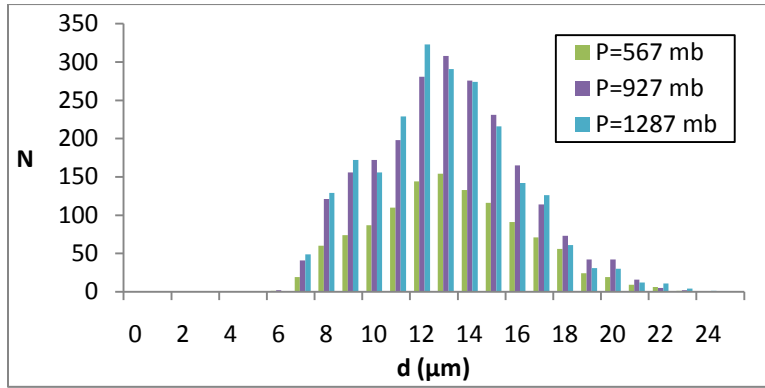


Fig. VII – Size distribution of nuclei measured by DIH in the range 5-25 μm

It must be pointed out that these distributions have been obtained by assuming the bubbles to be spherical. In fact, due to the circular shape of the point spread function (PSF) [13] and keeping in mind that the width of the PSF is roughly about 2 pixels, both non-spherical and spherical particles are seen as circular shape images. So, it is highly probable that other particles such as solid particles could wrongly have been identified as bubbles. This may lead to an overestimation of the concentration of small bubbles. This is good accordance with the conclusions of reference [17].

7.2. Range 12-140 μm

As mentioned in subsection 5.2, larger particles have been detected and measured individually. The montages of Fig. VIII show all the particle images that have been reconstructed, localized and measured in the range [12-140 μm] for three different pressures in the tunnel. For this representation, each image has been cropped by a square of 100x100 pixels around the particle image.

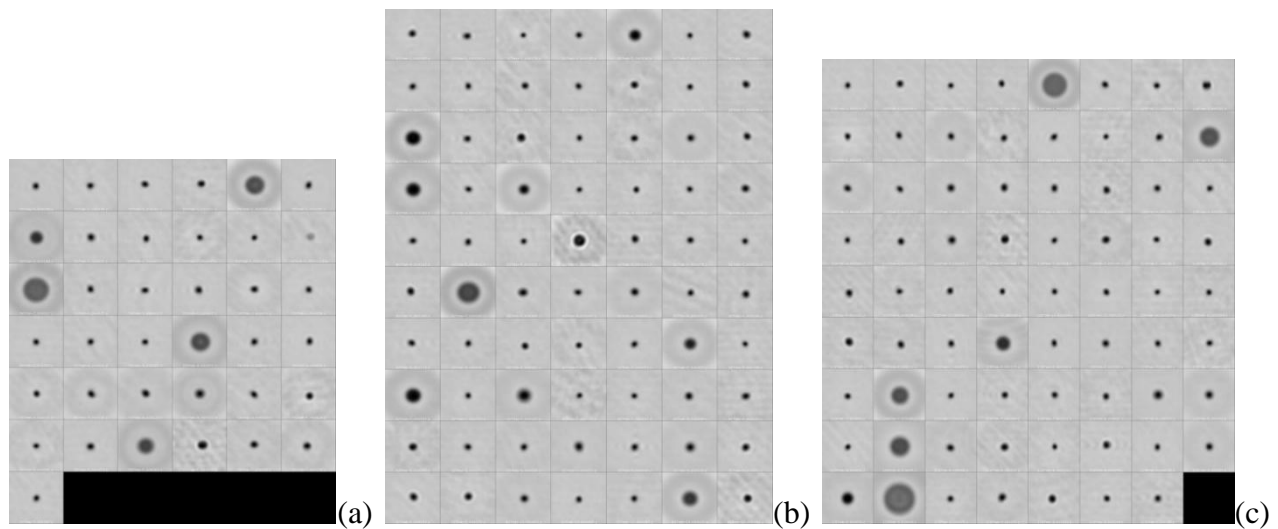


Fig. VIII – Images of bubbles reconstructed automatically from holograms in the range [12-140 μm]
 (a) $P = 567 \text{ mb}$, 1000 holograms (b), $P = 927 \text{ mb}$, 2000 holograms
 and (c) $P = 1287 \text{ mb}$, 2000 holograms

Here the image size is greater than the width of the PSF. As a result, it has been possible to reject non-spherical particles (fibers, solid particles ...) from the series of images. Fig. IX shows three examples of detected non-spherical particles that have been removed.

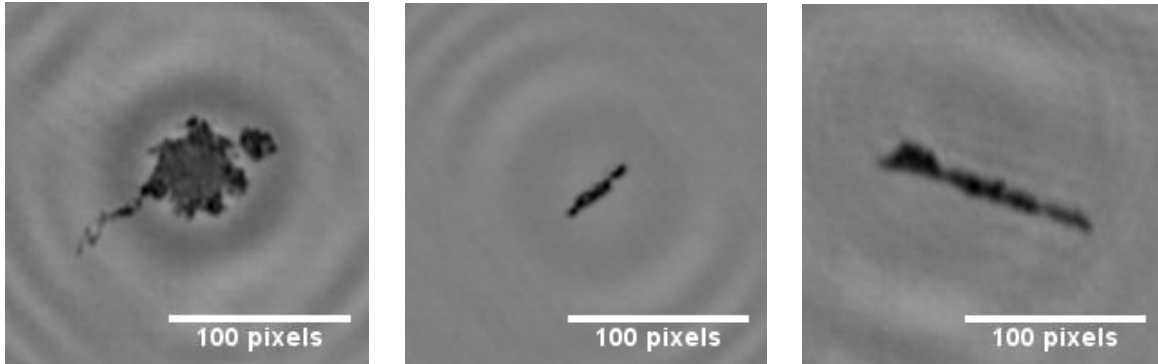


Fig. IX – Examples of non-spherical particles automatically extracted from the series

7.3. Synthesis 5-140 μm

Knowing the interrogation volume for each range, the concentration (bubble density in the optical pipe) has been evaluated. The results from both ranges are grouped together on figure X. We have checked that a given particle image were not twice counted on this diagram.

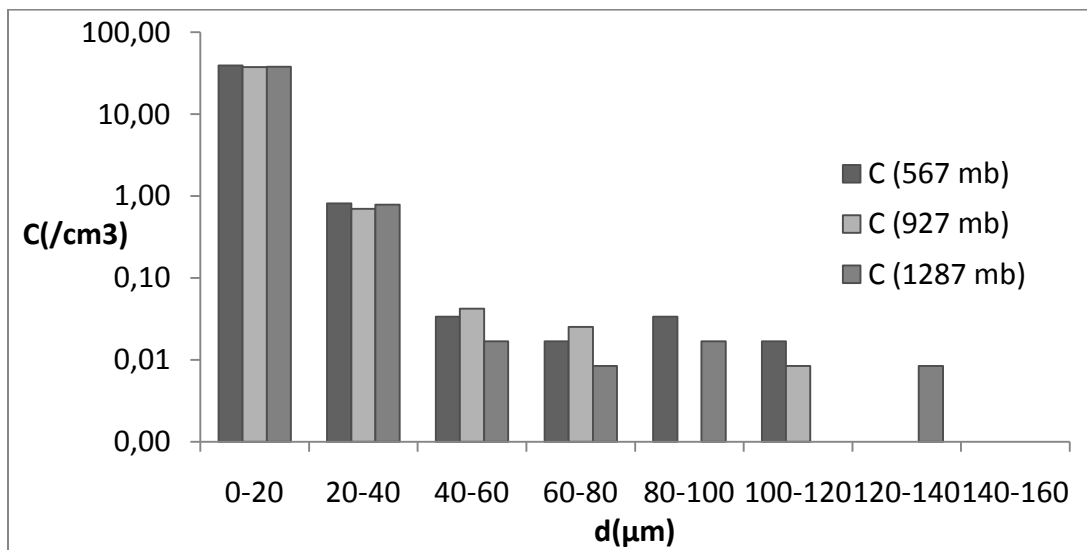


Fig X – Size nuclei distribution in the optical pipe for different flow pressures

It must be said that, due to the low concentration of bubbles in the upper range, the results obtained in the range 40-160 μm represent no more than 10 detected particles for a given condition. However, the

measured concentrations are in good accordance with the results obtained by other techniques (see ref. 17).

8. Conclusion

Digital in-line holography is applied to the measurement of bubble size in a cavitation tunnel. The optical magnification has been adapted to the size-range to be investigated (5-140 μm). A specific transparent pipe has been designed for this experiment. With this equipment, more than 5000 of holograms have been recorded and automatically processed by home-made software. Note that the focusing process differs as small or big particles are observed. This is why the ranges [5-25 μm] and [12-140 μm] have been studied separately. Concerning the upper range, non-spherical particles (like solid particles or fibers) can be detected and removed from the results. This work is to our knowledge the first study concerning statistical results of size measurement of bubbles by digital holography and processed by a fully automatic process. This makes possible a comparison with others (optical and non optical) measurement techniques.

9. References

1. Malek M, Lebrun D and Allano D, (2008), "Digital In-line holography system for 3D-3C Particle Tracking Velocimetry", A. Schröder, C.E. Willert (Eds.) : Particle Image Velocimetry, Topics Appl. Physics 112, pp 151-166
2. Garcia-Sucerquia J, Xu W, Jericho and Kreuzer HJ, (2006), "Immersion Digital in-line Holographic microscopy", Opt. Letters, Vol. 31 (9) , pp 1211-1213
3. Vikram CS and Billet ML, "Some salient features if in-line Fraunhofer holography with divergent beams", (1988), Optik, Vol. 78, pp 80-83
4. Tyler GA, Thompson BJ, (1976), "Fraunhofer holography Applied to Particle Size Analysis: A Reassessment", Opt. Acta, Vol. 23, pp 685-700.
5. Nicolas F, Coëtmelec S, Brunel M, Lebrun D, (2007) "Suppression of the moiré effect in sub-picosecond digital in-line holography", Opt. Express, Vol. 15, No. 3, pp 887-895.
6. Picart P and Leval J, (2008), "General theoretical formulation of image formation in digital Fresnel holography, JOSA, Vol. 25,7, pp 1744-1761
7. Kreis T, (2005), "Handbook of Holographic Interferometry, optical and Digital Methods", Wiley-VCH GmbH & Co. KGaA.
8. Zhang Y, Shen G, Schröder A, Kompenhans J, (2006), "Influence of some recording parameters on digital holographic particle image velocimetry", Opt. Eng. 45(7), pp 075801-10
9. Sheng J, Malkiel E and Katz J, (2006) "Digital holographic microscope for measuring three-dimensional particle distributions and motions", App. Optics, Vol. 45 (16), pp 3893-3901
10. Buraga C, Coëtmelec S, Lebrun D and Özkul C, (2000), "Application of wavelet transform to hologram analysis : three dimensional location of particles", Opt. and Lasers in Engineering, Vol 33 (6), pp 409-421
11. Verrier N, Coëtmelec S, Brunel M and Lebrun D, (2008), "Digital in-line holography in thick optical systems: application to visualization in pipes", App. Opt., Vol. 47, n°. 22, pp 4147-4157
12. Malek M, Coëtmelec S, Allano D and Lebrun D, (2003) "Formulation of in-line holography process by a linear shift invariant system: application to the measurement of fiber diameter", Opt. Comm., 223, pp 263-271

13. Pu SL, Allano D, Patte-Rouland B, Malek M, Lebrun D, and Cen KF, (2005), "Particle field characterization by digital in-line holography: 3D location and sizing", *exp. in fluids*,39, pp 1-9
14. Bexon R, Gibbs J and GD. Bishop, (1976), "Automatic assessment of aerosol holograms", *Journal of aerosol science*, Vol. 7, pp. 397-407
15. Meng H, Pan G, Pu Y and Woodward SH, (2004), "Holographic particle image velocimetry: from film to digital recording", *Meas. Sci. Technol.* Vol. 15, pp. 673-685
16. Salah N, Godard G, Lebrun D, Paranthoën P, Allano D and Coetmellec S, (2008) "Application of multiple exposure digital in-line holography to particle tracking in a Benard-von Karman vortex flow", *Meas. Sci. and Tech.*, Vol. 19, pp. 074001
17. Méès L, Lebrun D, Allano D, Walle F, Lecoffre Y, Boucheron R, Fréchou D (2010), "Development of interferometric techniques for nuclei size measurement in cavitation tunnel", 28th symposium on Naval Hydrodynamics, Pasadena, California, 12-17 september 2010.